Rapid volumetric angiography of cortical microvasculature with optical coherence tomography

Vivek J. Srinivasan,[1,*] James Y. Jiang,[2] Mohammed A. Yaseen,[1] Harsha Radhakrishnan,[1] Weicheng Wu,[1] Scott Barry,[2] Alex E. Cable,[2] and David A. Boas[1]

[1]*Photon Migration Imaging Laboratory, MGH/MIT/HMS Athinoula A. Martinos Center for Biomedical Imaging, Massachusetts General Hospital/Harvard Medical School, Charlestown, Massachusetts 02129, USA*

[2]*Thorlabs, Inc., Newton, New Jersey 07860, USA*

**Corresponding author: vjsriniv@nmr.mgh.harvard.edu*

Received October 9, 2009; revised November 23, 2009; accepted November 25, 2009; posted December 3, 2009 (Doc. ID 118166); published December 24, 2009

We describe methods and algorithms for rapid volumetric imaging of cortical vasculature with optical coherence tomography (OCT). By optimizing system design, scanning protocols, and algorithms for visualization of capillary flow, comprehensive imaging of the surface pial vasculature and capillary bed is performed in approximately 12 s. By imaging during hypercapnia and comparing with simultaneous CCD imaging, the sources of contrast of OCT angiography are investigated. © 2009 Optical Society of America

OCIS codes: 110.4500, 170.3880, 170.5380, 170.1470.

Cortical microvasculature is typically visualized *in vivo* by fluorescent labeling of blood plasma or red blood cells (RBCs) and optical imaging. Recently, high-speed spectral/Fourier domain optical coherence tomography (OCT) was used to visualize major cortical vessels by using intrinsic scattering contrast alone [1]. Moving and stationary tissue were separated by high-pass filtering along the fast axis of a raster scan. However, this approach requires dwell times approaching the millisecond time scale in order to visualize capillary flows [2]. When quantitative flow measurements are not required, the Nyquist frequency for sampling of a single transverse location may be less than the Doppler frequency shift. In this case, angiography measurements can be parallelized, enabling significant improvements in flow sensitivity and imaging speed. In this Letter, we present an OCT system along with methods and algorithms for rapid, high-resolution, volumetric angiography of cortical vasculature.

Animal protocols were approved by the animal care committee at Massachusetts General Hospital. Rats were prepared with cranial windows, immobilized stereotactically, and anesthetized with alphachloralose. A CCD camera with illumination at 570 nm (±5 nm) was employed for simultaneous imaging. A 1310 nm spectral/Fourier domain OCT microscope, shown in Fig. 1(A), was constructed for *in vivo* imaging of the rat cerebral cortex. The light source consisted of two superluminescent diodes combined by using a 50/50 fiber coupler to yield a bandwidth of 170 nm. The axial (depth) resolution was 4.7 μm in air (3.5 μm in tissue). The power on the sample was 4 mW, and the sensitivity was 105 dB. A spectrometer with a 1024 pixel InGaAs line scan camera operated at 47,000 axial scans/s. Either a 5× objective (7 μm transverse intensity profile FWHM at focus) or a 10× objective (3.5 μm transverse intensity profile FWHM at focus) was used. A line trigger from the InGaAs camera was used to synchronize the output of the galvanometer drive signals, ensuring that axial scans in repeated frames were acquired at the same transverse location. A real-time cross-sectional vascular imaging mode, discussed further below, enabled visualization of microvasculature in cross section and facilitated setting the focusing depth.

Figure 1(B) shows a scan protocol for volumetric angiography that samples the same transverse location twice per volume [3]. At 512 axial scans per image, each location is sampled at 11 ms intervals. A total of 1024 images at 512 y locations were acquired in 12 s to generate a single volumetric angiogram. (A conventional protocol [1] with a dwell time of 11 ms per location and 512×512=262,144 locations would require approximately 50 min, although faster imaging times of 10 s are possible by trading off velocity

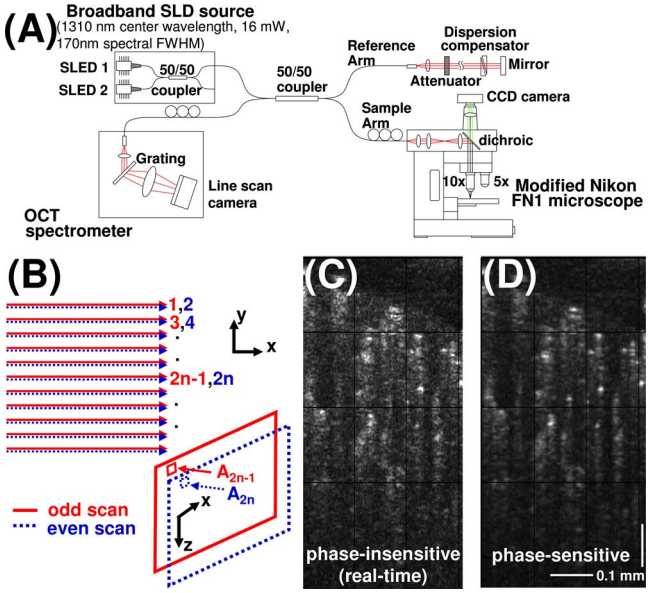

Fig. 1. (Color online) (A) OCT system and microscope schematic. (B) Three-dimensional scan protocol for performing OCT angiography that samples each transverse location twice. (C),(D) Examples of cross-sectional OCT angiograms generated by phase-insensitive and phase-sensitive methods described in the text.

sensitivity [4].) Sources of noise in the angiogram include photon shot noise and positional error. Sources of positional error include physiologic motion (heart rate, breathing rate), environmental vibrations, and galvanometer jitter. In general, transverse (x,y) positional error causes decorrelation [5], while axial (z) positional error causes a phase shift and decorrelation. Referring to Fig. 1(B) and neglecting the effects of shot noise, we use a simple model to describe the $(2n)$th complex signal A_{2n} in terms of the $(2n-1)$th complex signal A_{2n-1}, assuming no flow. The speckle correlation coefficient, $\alpha(\Delta x,\Delta y,\Delta z)$ is itself a random variable and depends on the positional shift $(\Delta x,\Delta y,\Delta z)$ between images. Therefore, $A_{2n}=\alpha(\Delta x,\Delta y,\Delta z)A_{2n-1}e^{j\Phi(\Delta z)}+N_{\text{decorr}}$. We estimate that $\alpha=0.98$ from our experimental measurements. Noting that $E[A_{2n-1}{}^{*}N_{\text{decorr}}]=0$ and $E[|A_{2n}|^2]=E[|A_{2n-1}|^2]=E[|A|^2]$, where $E[\ ]$ denotes expectation, we obtain that $E[|N_{\text{decorr}}|^2]=E[|A|^2](1-\alpha^2)$, showing that the severity of additive decorrelation noise depends on the local OCT signal power and α. $\Phi(\Delta z)=4\pi\Delta z/\lambda$ is a phase shift in the axial direction and is intrinsically related to an axial group delay shift and therefore speckle decorrelation. We estimate and correct for this phase shift by performing a cross correlation at every transverse (x,y) position. Then we take the difference as the angiogram: $|\Delta A_{\text{phase-sensitive}}|=|A_{2n,\text{corrected}}-A_{2n-1}|$. Assuming that it is possible to perfectly correct $\Phi(\Delta z)$, the baseline noise power is given by $E[|\Delta A_{\text{phase-sensitive}}|^2]=E[|A|^2](2-2\alpha)$. By equating the baseline noise power to $\Delta\Phi_{\text{Doppler}}{}^2E[|A|^2]$, the signal power due to a Doppler angle change of $\Delta\Phi_{\text{Doppler}}$, we calculate a minimum detectable Doppler phase shift of $(2-2\alpha)^{1/2}=0.2$ rad, corresponding to an axial velocity of 1.4 μm/s. The minimum velocities that cause decorrelation comparable with the baseline level ($\alpha=0.98$) are $\sim$40 μm/s (10$\times$ objective) and $\sim$80 μm/s (5$\times$ objective) in the transverse direction and $\sim$40 μm/s in the axial direction. In practice, these velocity sensitivities are achieved near the surface of the brain, where the shot-noise-limited signal-to-noise ratio is $>$17 dB, although lower velocity sensitivities are expected deeper in tissue where the signal-to-noise ratio is lower.

The approach presented here can be viewed as high-pass filtering along the raster scan slow axis as opposed to the conventional approach of high-pass filtering along the fast axis [1]. A related method for angiogram generation, used only for the real-time vascular imaging mode, is $|\Delta A_{\text{phase-insensitive}}|=||A_{2n}|-|A_{2n-1}||$. This method does not use phase information and is equivalent to high-pass filtering of the signal magnitude. Images generated by the phase-sensitive and phase-insensitive methods are shown in Figs. 1(C) and 1(D). Both methods use interframe analysis. Angiograms were displayed by averaging over 5 volumes, convoluting with a $3\times3\times3$ kernel, and summing the maximum 10–15 pixels at each transverse (x,y) position over selected depth regions. Applying a threshold based on an estimate of the local OCT signal power before the summing step further improves image quality.

Figure 2 shows a CCD image of a cranial window [Fig. 2(A)] and OCT angiogram [Fig. 2(B)] acquired with the 5$\times$ objective, enlargement of the OCT angiogram [Fig. 2(C)], and oblique slices through the volume [Fig. 2(D)] showing a stripe down the center of large vessels. The cross-sectional image at the location of the arrow (inset) shows a distinct pattern, with increased scattering toward the top and bottom of the vessel (solid arrows), and reduced scattering at the sides (dotted arrows). This pattern may be due to orientation dependence of backscattering from RBCs [6] and their tendency to orient parallel to the vessel wall in high shear flows [7]. Therefore, the RBCs at the top and bottom of the vessel have a larger backscattering cross section than the RBCs at the sides of the vessel, possibly explaining the stripe pattern.

Figure 3 shows imaging of the response to hypercapnia using the 10$\times$ objective with 15 s temporal resolution. Pa_{CO_2} increased from 35.7 mmHg during normocapnia to 57.5 mmHg after 7 min of inhalation of a breathing mixture with 7.5% CO_2. Figure 3(A) shows the baseline CCD image, and Fig. 3(B) shows the baseline OCT angiogram over a depth range from the cortical surface to 330 μm. The CCD image and the OCT angiogram show similar vasculature. One notable exception is the vessel segment circled in Fig. 3(A) (inset). This vessel segment contains RBCs, but the transverse flow in this vessel is quasi-static and occasionally reverses direction ($<$25 μm/s as determined by CCD imaging), and the axial component presumably does not exceed the threshold for OCT detection. Therefore, no signal is seen at the corresponding location in the OCT angiogram circled in Fig. 3(B) (inset). Figure 3(C) shows the diameters of an artery (A) and a vein (V) with similar calibers [labeled in Fig. 3(B)] during CO_2 inhalation, denoted by

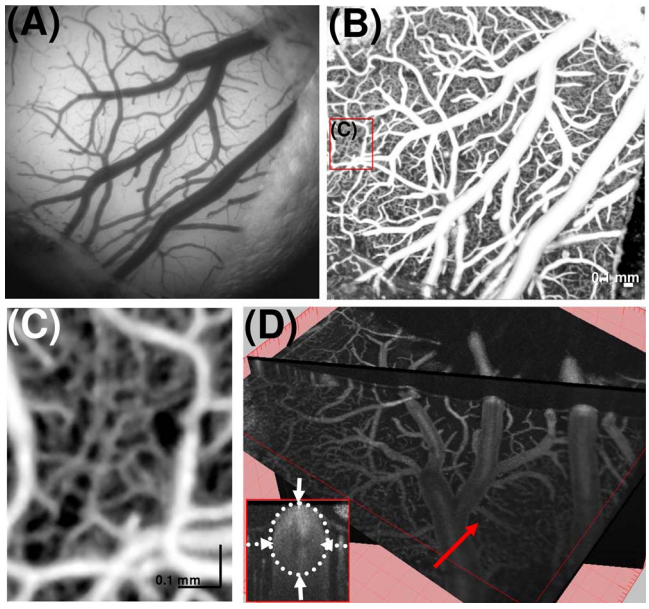

Fig. 2. (Color online) (A) CCD image and (B) wide-field OCT angiogram of cranial window with (C) enlargement showing microvasculature. (D) 3D oblique slices and cross-sectional image (inset) showing distinct backscattering pattern due to shear-induced orientation of RBCs.

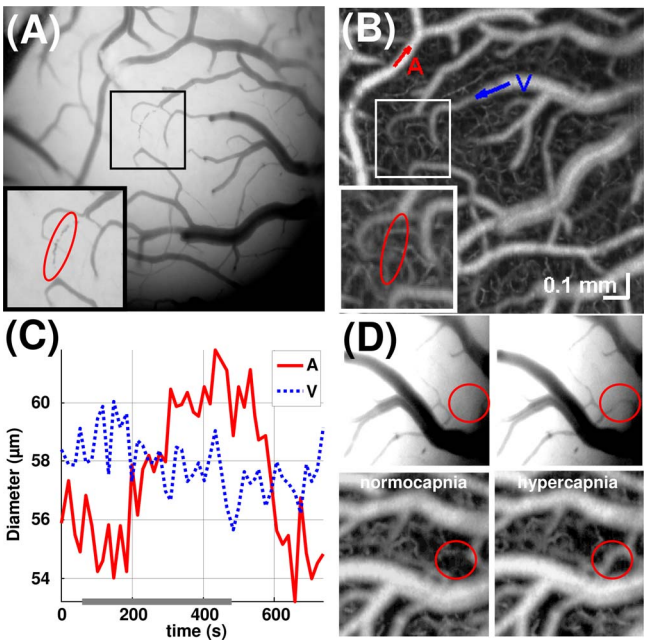

Fig. 3. (Color online) (A) CCD image and (B) OCT angiogram of cortical vasculature during normocapnia. (C) Changes in vessel tone in representative artery A and vein V during 7.5% hypercapnia, shown as a line along the time axis. (D) Transient perfusion of arterial anastomosis during hypercapnia visualized by CCD imaging (above) and confirmed by OCT (below).

a thick line along the time axis. Figure 3(D) shows an enlargement of the surface vasculature, showing a circled arterial anastomosis during normocapnia and hypercapnia imaged by the CCD camera (above) and by OCT (below). The CCD image shows the anastomosis fill with blood during hypercapnia resulting in increased absorption at this location. The OCT angiogram, based on flow and scattering contrast, shows a brightening of this area, indicating perfusion. Figure 4 shows OCT angiograms of the capillary bed over a depth range from 330 to 510 μm during normocapnia [Figs. 4(A) and 4(C)] and hypercapnia [Figs. 4(B) and 4(D)]. A reorganization of capillary flow is observed. For instance, the location marked by the dotted arrow brightens during hypercapnia, while the location marked by the solid arrow darkens during hypercapnia. These results are consistent with a redistribution of capillary perfusion during hypercapnia [8].

Caution must be exercised in the interpretation of OCT angiograms. The contrast of this and related methods [1,9] arises from scattering of moving RBCs. Therefore, an increase in angiogram intensity may be due to an increase in RBC velocity above a threshold or an increase in backscattering resulting from an increase in hematocrit or a change in RBC orientation. A coregistered Doppler measurement of velocity as well as OCT signal magnitude would help to resolve this ambiguity. Additionally the effect of scattering changes in superficial layers on imaging of deeper layers cannot be discounted. Finally, in spectral/Fourier domain OCT, the camera integration time preferentially weights lower velocities, thus acting as a low-pass filter. This analog low-pass filter may be compensated by designing an appropriate digital inverse filter.

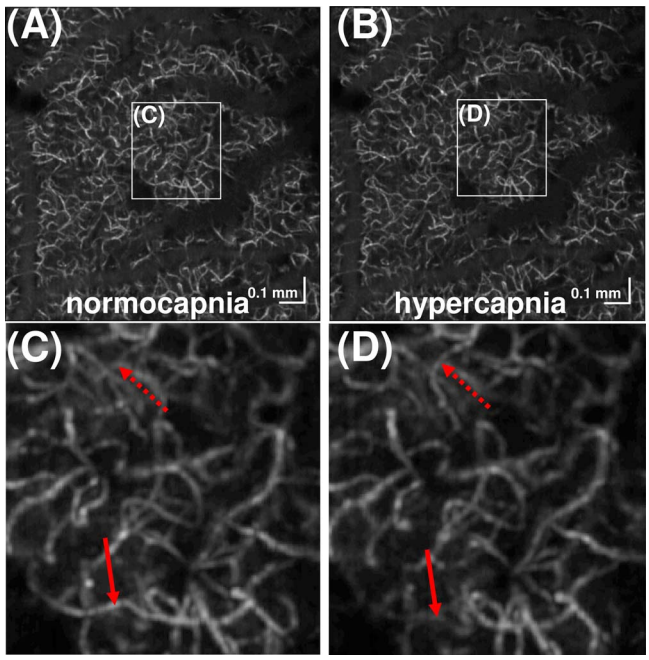

Fig. 4. (Color online) (A), (C), Media 1: OCT imaging of the capillary bed during normocapnia. (B), (D), Media 2: hypercapnia, demonstrating flow redistribution (arrows).

In conclusion, we demonstrate rapid volumetric OCT angiography of surface and parenchymal vasculature through cranial windows. In addition to providing qualitative information on perfusion, these methods may be used to quantitatively measure changes in vessel tone. Therefore, these optical techniques and algorithms may have important applications in the study of cerebrovascular reactivity and experimental stroke models.

We acknowledge support by the National Institutes of Health (NIH) (R01-NS057476, P01NS055104, P50NS010828, and K99NS067050) and the Air Force Office of Scientific Research (AFOSR) (MFEL FA9550-07-1-0101).

References

1. R. K. Wang, S. L. Jacques, Z. Ma, S. Hurst, S. R. Hanson, and A. Gruber, Opt. Express **15**, 4083 (2007).
2. Y. K. Tao, A. M. Davis, and J. A. Izatt, Opt. Express **16**, 12350 (2008).
3. J. Fingler, D. Schwartz, C. Yang, and S. E. Fraser, Opt. Express **15**, 12636 (2007).
4. R. K. Wang and L. An, Opt. Express **17**, 8926 (2009).
5. B. J. Vakoc, G. J. Tearney, and B. E. Bouma, IEEE Trans. Med. Imaging **28**, 814 (2009).
6. A. M. Nilsson, P. Alsholm, A. Karlsson, and S. Andersson-Engels, Appl. Opt. **37**, 2735 (1998).
7. H. Schmid-Schoenbein and R. Wells, Science **165**, 288 (1969).
8. E. B. Hutchinson, B. Stefanovic, A. P. Koretsky, and A. C. Silva, Neuroimage **32**, 520 (2006).
9. A. Mariampillai, B. A. Standish, E. H. Moriyama, M. Khurana, N. R. Munce, M. K. Leung, J. Jiang, A. Cable, B. C. Wilson, I. A. Vitkin, and V. X. Yang, Opt. Lett. **33**, 1530 (2008).